**Finely tuning electrolytes and photoanodes in aqueous solar cells by experimental design**

# Finely tuning electrolytes and photoanodes in aqueous solar cells by experimental design

Simone **Galliano**,[1] Federico **Bella**,[2,*] Giulia **Piana**,[2] Giulia **Giacona**,[1,2] Guido **Viscardi**,[1] Claudio **Gerbaldi**,[2] Michael **Grätzel**,[3] Claudia **Barolo**[1,4,*]

*1) Department of Chemistry, NIS Interdepartmental Centre and INSTM Reference Centre, Università degli Studi di Torino, Via Pietro Giuria 7, 10125 - Torino, Italy*

*2) GAME Lab, Department of Applied Science and Technology - DISAT, Politecnico di Torino, Corso Duca degli Abruzzi 24, 10129 – Torino, Italy*

*3) Laboratory of Photonics and Interfaces, Institut des Sciences et Ingénierie Chimiques, Ecole Polytechnique Fédérale de Lausanne (EPFL), Station 3, CH1015 – Lausanne, Switzerland*

*4) ICxT Interdepartmental Centre, Università degli Studi di Torino, Lungo Dora Siena 100, 10153 – Torino, Italy*

**Corresponding authors**: Federico Bella (federico.bella@polito.it, +39 0110904643) and Claudia Barolo (claudia.barolo@unito.it, +39 0116707594).

**Abstract**: If opportunely developed and optimized, aqueous dye-sensitized solar cells can be considered a truly low impact photovoltaic device, with no toxic components. Here we report the use of design of experiments as a useful chemometric technique for the concurrent investigation of a series of experimental factors that directly influence the proper operation of these photoelectrochemical cells. Results obtained enlighten that a solid mathematical-statistical approach is fundamental to support the researchers and effectively drive the experiments towards the achievements of optimal operating conditions of any new energy device, thus bypassing the energy/time consuming of traditional monovariate one-factor-at-a-time method.

**Keywords**: Dye-sensitized solar cell; Aqueous electrolyte; Sustainability; Design of experiments; Multivariate approach; Electrode/electrolyte interface.

## 1. Introduction

The introduction of aqueous electrolytes is contributing to the rebirth of dye-sensitized solar cells (DSSCs), the low-impact photoelectrochemical device for the conversion of solar energy into electricity (Bella et al., 2015). Aqueous DSSCs represent a truly sustainable and very limited environmental impact technology, which might successfully pinpoint the concept of artificial photosynthesis often been evoked within

the scientific community in the last two decades (Bella et al., 2017; Click et al., 2017; Imperiyka et al., 2014; McConnell et al., 2010; Yang et al., 2010).

Several research groups worldwide recently focused their efforts towards the investigation of a series of new factors, such as photoelectrode wetting (Dong et al., 2014; Galliano et al., 2017), novel sensitizers (Leandri et al., 2014; Li et al., 2017; Lin et al., 2015), the solubility and the diffusion behavior of various redox pairs in water (Daeneke et al., 2012; Xiang et al., 2013; Yang et al., 2015), the cathodic electrocatalytic reaction (Ellis et al., 2016). Clearly, in a new system (like the aqueous DSSC), the possibility to simultaneously study several of these experimental factors at the same time, bypassing the traditional one-factor-at-a-time (OFAT) process, would permit to effectively drive research towards well-defined paths supported by a solid mathematical/statistical justification. In this respect, despite being scarcely adopted by the energy-related research community (Gianotti et al., 2014; Miccoli et al., 2016), multivariate chemometrics, such as design of experiments (DoE) (Kennard et al., 1969), would represent a key-enabling method.

In this work, we propose a DoE for the simultaneous investigation of the characteristics of photoanode, electrolyte and photoanode/electrolyte interface of aqueous DSSCs. A simple experimental matrix based on 20 photoelectrochemical cells enables to comprehensively weight each of the experimental factors involved, and to easily identify the best conditions to maximize sunlight conversion efficiency. Amongst the powerful and intriguing aspects of the adopted approach, the ability to find two performance maximization strategies must be mentioned, which is the fundamental achievement of this work.

## 2. Experimental

Sodium iodide (NaI), iodine ($I_2$), chenodeoxycholic acid (CDCA), ethanol, acetone, *tert*-butanol (*t*-BuOH) and acetonitrile (ACN) were purchased from Sigma-Aldrich. Deionized water (DI-$H_2O$, 18 MΩ $cm^{-1}$ at 25 °C) was obtained by Direct-Q 3 UV Water Purification System (Millipore). Sensitizing dye 2-[{4-[4-(2,2-diphenylethenyl)phenyl]-1,2,3,3a,4,8b-hexahydrocyclopento[b]indole-7-yl}methylidene]-cyanoacetic acid (D131) was purchased from Inabata Europe S.A. FTO-glass plates (sheet resistance 7 Ω $sq^{-1}$, purchased from Solaronix) were cut into 2 cm × 1.5 cm sheets and used as substrates for the fabrication of both photoanodes and counter electrodes.

FTO covered glasses were rinsed in mixed acetone/ethanol in an ultrasonic bath for 10 min; solvent traces were removed by flash evaporation at 450 °C on a hotplate. Front electrodes were prepared by depositing a single layer of porous $TiO_2$ on top of the conductive substrate by means of a manual screen printer with a 43T mesh frame. After deposition of the paste (18NR-T, Dyesol) and 20 min rest to let it bed thoroughly, the $TiO_2$ layer was dried at 80 °C for 20 min; finally, it was sintered increasing the temperature up to 480 °C in 45 min. The fabricated photoanodes had a thickness of ≈6 μm and active area of 0.25 $cm^2$. They were finally reactivated by heating at 450 °C for 20 min and, subsequently, soaked into a D131 dye solution (0.50 mM in *t*-BuOH:ACN 1:1); CDCA was added to the dye solution as coadsorbent (its concentration represents one of the factors investigated in this work). Dipping in dye solutions was carried out at 22 °C for 5 h under dark conditions and shaking in a Buchi Syncore platform equipped with a cooling plate. After dye loading, photoanodes were washed in acetone to remove residual dye not specifically adsorbed onto the $TiO_2$ layer.

As regards the preparation of counter electrodes, FTO conductive glasses were platinized by spreading a $H_2PtCl_6$ 5.0 mM solution on the plate surface and heating up to 400 °C.

Photoanodes were faced to the counter electrodes exploiting Surlyn® thermoplastic frames (internal area 0.6 cm × 0.6 cm) as spacers (60 μm thick), taking care of the overlapping of the active areas. All of these components were assembled by hot pressing (20 s) at 110 °C. The electrolyte solution (consisting of NaI and $I_2$ dissolved in water) was injected by vacuum backfilling process through a hole in the Surlyn® frame, which was then sealed by a commercial epoxy glue. The amounts of NaI and $I_2$ represent relevant factors in the aqueous DSSC field, thus they are investigated in this work.

Photovoltaic performances were evaluated recording three consecutive $J-V$ curves on a Keithley 2420 Source Measure Unit. Cells were irradiated under simulated 1 sun light intensity (100 mW $cm^{-2}$, AM 1.5G) after calibration by silicon diode, as it is typically done in the DSSC framework (Bella et al., 2017; Fan et al., 2017; Liu et al., 2017; Maçaira et al., 2017; Mengal et al., 2017). Electrochemical impedance spectroscopy (EIS) data were recorded using a potentiostat (CH Instruments Inc., Model 680) in the frequency range between 10 kHz and 0.1 Hz. The amplitude of the AC signal was 10 mV. Spectra were recorded under dark conditions at applied DC potentials equal to the previously measured $V_{oc}$ values under 1 sun (Buraidah et al., 2017; Mohan et al., 2017; Paušová et al., 2017; Subramanian et al., 2017; Vekariya et al., 2017).

## 3. Results and Discussion

An experimental design was compiled to simultaneously investigate the effect of two key parameters, such as the concentration of the redox mediator and the ratio between the co-adsorbent CDCA and the dye-sensitizer in the photoanode dipping solution, of an aqueous DSSC. As regards the electrolyte, two variables were identified: concentrations of $I_2$ ($x_2$, from 10 to 30 mM) and NaI ($x_3$, from 1.0 to 5.0 M), respectively. The CDCA/Dye molar ratio ($x_1$) was the third variable, which ranged from 18 to 50. Such an experimental domain was chosen accordingly to preliminary tests useful to identify the most appropriate conditions to enable proper operation of lab-scale aqueous DSSCs (Bella et al., 2016). In order to carry out a multivariate experimental design, the software MODDE (version 11.0.2.2309, Umetrics) was chosen. A two-level full factorial DoE was planned and the list of experiments is summarized in **Table 1**, together with the measured responses of short-circuit current density ($J_{sc}$), open-circuit potential ($V_{oc}$), fill factor (FF) and power conversion efficiency (PCE) (Abdul Rani et al., 2014; Park et al., 2015). These experiments represent the most statistically significant points of the investigated experimental domain as a whole, and design the cubic geometry shown in **Fig. A.1 in Appendix A**.

**Table 1.** DoE model matrix consisting of 20 experiments, useful to investigate the three selected experimental variables ($x_1$, $x_2$ and $x_3$). The measured responses for $J_{sc}$, $V_{oc}$, FF and PCE are also shown.

| Exp. | CDCA:Dye ratio [$x_1$] | [Iodine] ($x_2$, mM) | [Iodide] ($x_3$, M) | $J_{sc}$ (mA cm$^{-2}$) | $V_{oc}$ (mV) | FF (%) | PCE (%) |
|---|---|---|---|---|---|---|---|
| **N1** | 18:1 | 10 | 1.0 | 1.48 | 564 | 54.7 | 0.46 |
| **N2** | 50:1 | 10 | 1.0 | 2.21 | 607 | 54.7 | 0.73 |
| **N3** | 18:1 | 30 | 1.0 | 0.92 | 476 | 54.9 | 0.24 |
| **N4** | 50:1 | 30 | 1.0 | 1.71 | 540 | 59.5 | 0.55 |
| **N5** | 18:1 | 10 | 5.0 | 3.55 | 528 | 56.0 | 1.05 |
| **N6** | 50:1 | 10 | 5.0 | 1.73 | 532 | 44.2 | 0.41 |
| **N7** | 18:1 | 30 | 5.0 | 2.67 | 450 | 58.3 | 0.70 |
| **N8** | 50:1 | 30 | 5.0 | 2.27 | 465 | 45.6 | 0.48 |

| | | | | | | | |
|---|---|---|---|---|---|---|---|
| **N9** | 34:1 | 20 | 3.0 | 0.70 | 425 | 53.4 | 0.17 |
| **N10** | 34:1 | 20 | 3.0 | 1.35 | 453 | 56.9 | 0.35 |
| **N11** | 18:1 | 10 | 1.0 | 1.56 | 549 | 55.6 | 0.48 |
| **N12** | 50:1 | 10 | 1.0 | 2.57 | 613 | 57.1 | 0.90 |
| **N13** | 18:1 | 30 | 1.0 | 1.08 | 494 | 57.3 | 0.30 |
| **N14** | 50:1 | 30 | 1.0 | 1.88 | 557 | 59.7 | 0.63 |
| **N15** | 18:1 | 10 | 5.0 | 3.47 | 502 | 56.1 | 0.98 |
| **N16** | 50:1 | 10 | 5.0 | 1.72 | 534 | 44.0 | 0.42 |
| **N17** | 18:1 | 30 | 5.0 | 2.82 | 434 | 58.2 | 0.71 |
| **N18** | 50:1 | 30 | 5.0 | 2.58 | 474 | 44.6 | 0.55 |
| **N19** | 34:1 | 20 | 3.0 | 1.12 | 463 | 56.2 | 0.29 |
| **N20** | 34:1 | 20 | 3.0 | 1.44 | 468 | 57.8 | 0.39 |

The model was fitted with the obtained experimental responses listed in **Table 1** and the *summary of fit* plot, i.e. a bar graph showing the values of the $R^2$, $Q^2$ and reproducibility parameters, is shown in **Fig. A.2 in Appendix A**. By the analysis of the data, it is evidenced that the resulting regression model provides a significant description of the relationship between the independent variables and the responses, which means an optimal analysis of the investigated photoelectrochemical system, as also shown in **Fig. A.3 in Appendix A**.

To figure out the most significant within all of the variables under study, a *coefficients plot* for the selected response was elaborated as shown in **Fig. 1**. We noticed that the increase in the concentration of $I_2$ and NaI negatively affected the $V_{oc}$, while the opposite effect was obtained by raising CDCA concentration. On the contrary, $J_{sc}$ values increased upon NaI addition, unless when also CDCA was added in high amounts. Overall, the PCE substantially increased at increasing amounts of NaI, while decreased upon increasing the concentration of $I_2$. The worst situation is highlighted by the interaction coefficient $x_1 \times x_3$, i.e. when concentration levels of CDCA and NaI are kept both at the highest level. **Fig. 1** truly helps in identify the most relevant

experimental factors affecting each of the photovoltaic parameters measured by $J-V$ analysis.

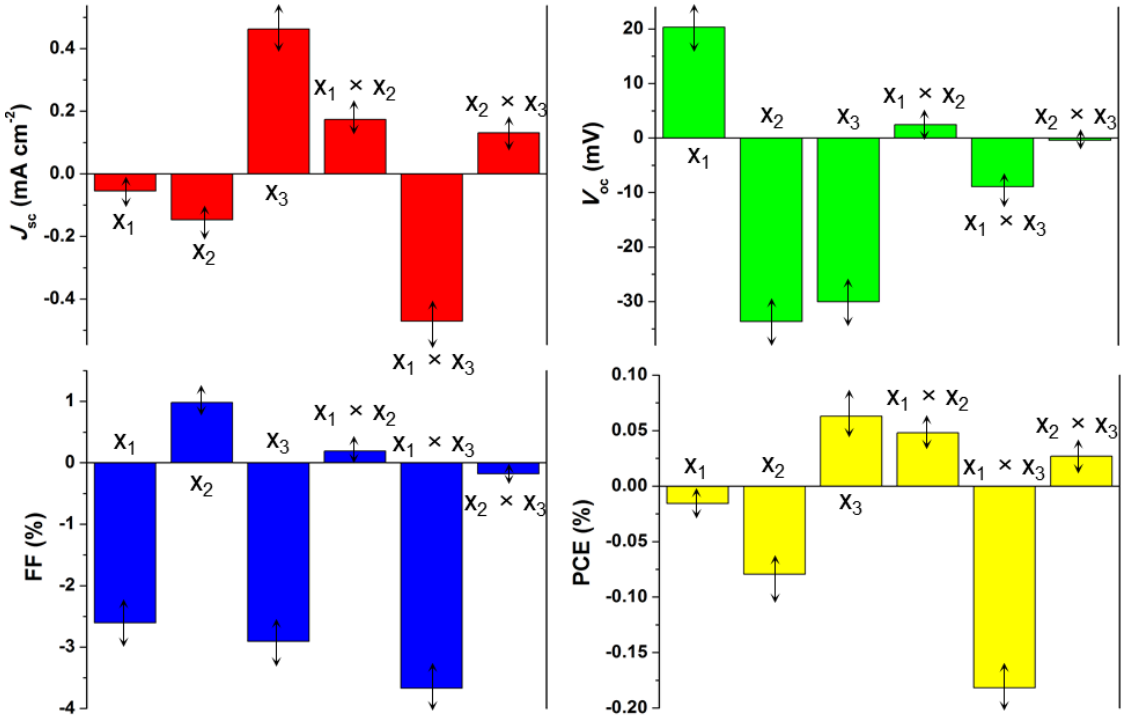


**Fig. 1**. *Coefficient plot* for the DoE. Each plot displays the coefficients, when changing from level 0 to a higher level, for the selected response (i.e., the photovoltaic parameters).

*Contour plots* (isoresponse graphs) are shown in **Fig. 2** (for $J_{sc}$, $V_{oc}$ and PCE) and in **Fig. A.4 in Appendix A** (for FF). They graphically show the relevance of each factor in influencing the measured response. In particular, highest values of $V_{oc}$ were obtained at low concentrations of NaI and $I_2$ ad high amount of CDCA. This was due to the inhibition of electron–$I_2$ and electron–$I_3^-$ recombination processes usually observed in $I_2$-rich electrolytes (Mathew et al., 2013); moreover, it is known from Nernst equation that an increase in NaI concentration reduces the working potential value (Fabregat-Santiago et al., 2005).

166

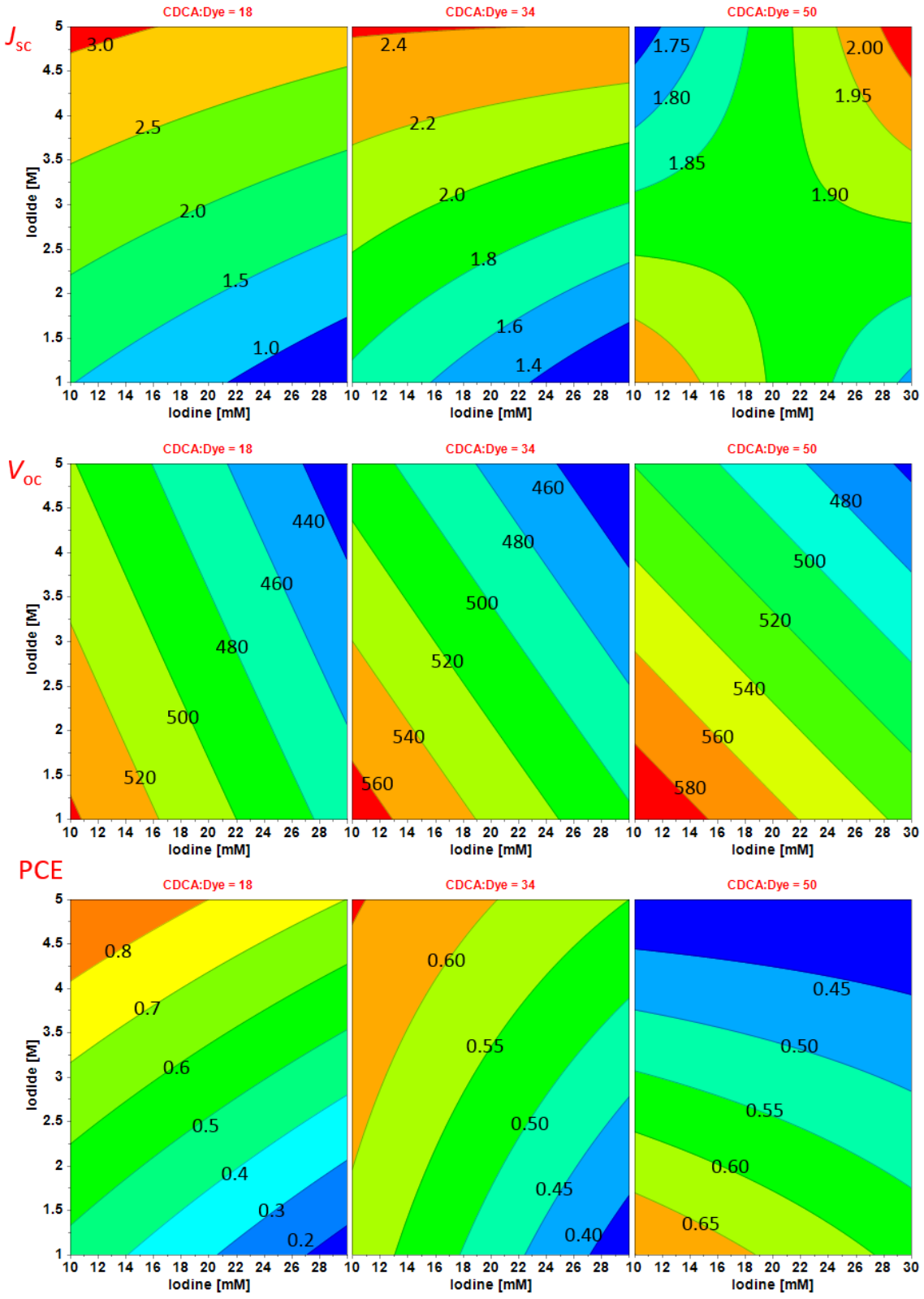
$J_{SC}$
CDCA:Dye = 18
CDCA:Dye = 34
CDCA:Dye = 50
3.0
2.5
2.0
1.5
1.0
2.4
2.2
2.0
1.8
1.6
1.4
1.75
1.80
1.85
1.90
1.95
2.00
$V_{OC}$
440
460
480
500
520
460
480
500
520
540
560
480
500
520
540
560
580
PCE
0.8
0.7
0.6
0.5
0.4
0.3
0.2
0.60
0.55
0.50
0.45
0.40
0.45
0.50
0.55
0.60
0.65
Iodide [M]
Iodine [mM]

167

**Fig. 2.** *Contour plots* of the fitted DoE considering $J_{sc}$, $V_{oc}$ and PCE as response; their values are written onto the contour lines. Values range from low (blue) to high (red) values.

As regards $J_{sc}$, in the presence of medium-low CDCA:Dye ratios the maximum current density values were achieved at high NaI content, with a rather little effect given by the selected concentration of $I_2$. Conversely, at high CDCA:Dye ratios, $J_{sc}$ trend showed two maxima: i) at low [NaI] and [$I_2$], and ii) at high [NaI] and [$I_2$] values, respectively. Also PCE values showed a peculiar trend, with high values obtained in the presence of low $I_2$ and high NaI contents at medium-low CDCA:Dye ratios, while the best PCE values resulted at high CDCA levels in the presence of low concentrations of iodine species. This performance trend is basically related to the amount of dye molecules anchored at the surface of the $TiO_2$ electrode. Actually, at low dye loading (high ratio CDCA:Dye), little amounts of iodide ions are sufficient for the regeneration of the oxidized sensitizer molecules; conversely, at low CDCA:Dye ratios, increased iodide concentration is required to enable the efficient reduction of $Dye^+$ species.

*Contour plots* clearly show the advantages of the DoE approach in the rapid and effective characterisation of an electrochemical power source, highlighting that device performance can be maximized by different combinations of the same experimental parameters. **Fig. 3** shows the *J*–*V* and Nyquist plots of N5 and N12, which are the two best cells of the experimental matrix detailed in **Table 1**. Clearly, even if the two cells provided similar PCE values (1.05% and 0.90%, respectively), their figure of merits are rather different. Indeed, cell N5 shows high $J_{sc}$, low $V_{oc}$, recombination resistance ($R_{ct}$ = 82.5 Ω) and redox couple diffusion resistance ($R_d$ = 23.3 Ω) as expected for DSSCs based on liquid electrolytes containing high amount of iodine species; conversely, the

lower redox mediator content in cell N12 leads to lower $J_{sc}$, higher $V_{oc}$, $R_{ct}$ (154 Ω) and $R_d$ (44.4 Ω).

In our opinion, the experimental conditions adopted for cell N12 are preferable than those of cell N5, since the use of lower amounts of dye and redox mediator would lower the final cost of the solar cell, without affecting the overall sunlight conversion efficiency.

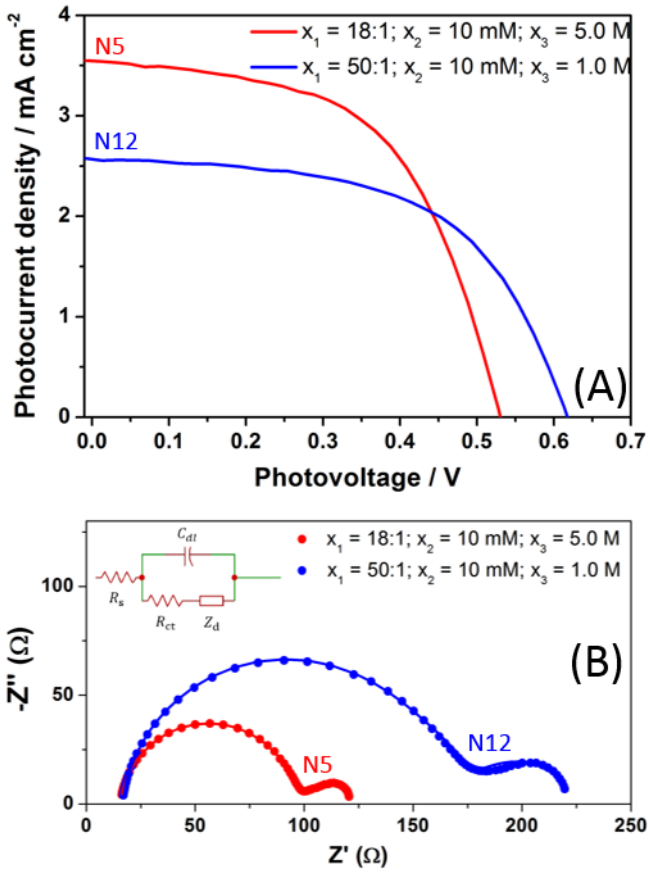


**Fig. 3.** (A) *J–V* curves and (B) corresponding Nyquist plots of aqueous DSSCs (N5 and N12 of **Table 1**) measured under 1 sun irradiation (AM 1.5G). Inset of B) represents the equivalent circuit used to fit experimental data.

## 4. Conclusions

A multivariate study of photoelectrode sensitization, electrolyte formulation and interface phenomena in aqueous DSSCs has been proposed in this work. The proposed

approach enlightened that the concurrent evaluation of several experimental factors affecting the overall performance is fundamental to support the researchers in finding the optimal operating conditions of any new energy device with solid mathematical and statistical bases (Ccorahua et al., 2017; D'Angelo et al., 2017; Feng et al., 2017; Miao et al., 2017; Zhu et al., 2017). The lab-scale aqueous DSSCs, that were assembled based on the optimised parameters resulting for chemometrics, provided a reproducible ≈1% sunlight conversion efficiency without the addition of additives, and can therefore be used as a solid benchmark for future studies aimed at boosting its performance.

**Acknowledgements**

This research did not receive any specific grant from funding agencies in the public, commercial, or not-for-profit sectors.

**References**

Abdul Rani, R., Zoolfakar, A.S., Subbiah, J., Ou, J.Z., Kalantar-Zadeh, K., 2014. Highly ordered anodized $Nb_2O_5$ nanochannels for dye-sensitized solar cells. Electrochem. Commun. 40, 20-23.

Bella, F., Gerbaldi, C., Barolo, C., Grätzel, M., 2015. Aqueous dye-sensitized solar cells. Chem. Soc. Rev. 44, 3431-3473.

Bella, F., Galliano, S., Falco, M., Viscardi, G., Barolo, C., Grätzel, M., Gerbaldi, C., 2016. Unveiling iodine-based electrolytes chemistry in aqueous dye-sensitized solar cells. Chem. Sci. 7, 4880-4890.

Bella, F., Popovic, J., Lamberti, A., Tresso, E., Gerbaldi, C., Maier, J., 2017. Interfacial effects in solid-liquid electrolytes for improved stability and performance of dye-sensitized solar cells. ACS Appl. Mater. Interfaces 9, 37797-37803.

Bella, F., Verna, A., Gerbaldi, C., 2018. Patterning dye-sensitized solar cell photoanodes through a polymeric approach: A perspective. Mater. Sci. Semicond. Process. 73, 92-98.

Buraidah, M.H., Shah, S., Teo, L.P., Chowdhury, F.I., Careem, M.A., Albinsson, I., Mellander, B.-E., Arof, A.K., 2017. High efficient dye sensitized solar cells using phthaloylchitosan based gel polymer electrolytes. Electrochim. Acta 245, 846-853.

Ccorahua, R., Troncoso, O.P., Rodriguez, S., Lopez, D., Torres, F.G., 2017. Hydrazine treatment improves conductivity of bacterial cellulose/graphene nanocomposites obtained by a novel processing method. Carbohydr. Polym. 171, 68-76.

Click, K.A., Schockman, B.M., Dilenschneider, J.T., McCulloch, W.D., Garrett, B.R., Yu, Y., He, M., Curtze, A.E., Wu, Y., 2017. Bilayer dye protected aqueous photocathodes for tandem dye-sensitized solar cells. J. Phys. Chem. C 121, 8787-8795.

D'Angelo, A.J., Panzer, M.J., 2017. Enhanced lithium ion transport in poly(ethylene glycol) diacrylate-supported solvate ionogel electrolytes via chemically cross-linked ethylene oxide pathways. J. Phys. Chem. B 121, 890-895.

Daeneke, T., Uemura, Y., Duffy, N.W., Mozer, A.J., Koumura, N., Bach, U., Spiccia, L., 2012. Aqueous dye-sensitized solar cell electrolytes based on the ferricyanide-ferrocyanide redox couple. Adv. Mater. 24, 1222-1225.

Dong, C., Xiang, W., Huang, F., Fu, D., Huang, W., Bach, U., Cheng, Y.B., Li, X., Spiccia, L., 2014. Controlling interfacial recombination in aqueous dye-sensitized solar cells by octadecyltrichlorosilane surface treatment. Angew. Chem. Int. Ed. 53, 6933-6937.

Ellis, H., Jiang, R., Ye, S., Hagfeldt, A., Boschloo, G., 2016. Development of high efficiency 100% aqueous cobalt electrolyte dye-sensitised solar cells. Phys. Chem. Chem. Phys. 18, 8419-8427.

Fabregat-Santiago, F., Bisquert, J., Garcia-Belmonte, G., Boschloo, G., Hagfeldt, A., 2005. Influence of electrolyte in transport and recombination in dye-sensitized solar cells studied by impedance spectroscopy. Sol. Energy Mater. Sol. Cells 87, 117-131.

Fan, K., Yu, J., Ho, W., 2017. Improving photoanodes to obtain highly efficient dye-sensitized solar cells: A brief review. Mater. Horiz. 4, 319-344.

Feng, X., Yang, Z., Chmely, S., Wang, Q., Wang, S., Xie, Y., 2017. Lignin-coated cellulose nanocrystal filled methacrylate composites prepared via 3D stereolithography printing: Mechanical reinforcement and thermal stabilization. Carbohydr. Polym. 169, 272-281.

Galliano, S., Bella, F., Gerbaldi, C., Falco, M., Viscardi, G., Grätzel, M., Barolo, C., 2017. Photoanode/electrolyte interface stability in aqueous dye-sensitized solar cells. Energy Tech. 5, 300-311.

Gianotti, V., Favaro, G., Bonandini, L., Palin, L., Croce, G., Boccaleri, E., Artuso, E., Van Beek, W., Barolo, C., Milanesio, M., 2014. Rationalization of dye uptake on titania slides for dye-sensitized solar cells by a combined chemometric and structural approach. ChemSusChem 7, 3039-3052.

Imperiyka, M., Ahmad, A., Hanifah, S.A., Bella, F., 2014. A UV-prepared linear polymer electrolyte membrane for dye-sensitized solar cells. Physica B 450, 151-154.

Kennard, R.W., Stone, L.A., 1969. Computer aided design of experiments. Technometrics 11, 137-148.

Leandri, V., Ellis, H., Gabrielsson, E., Sun, L., Boschloo, G., Hagfeldt, A., 2014. An organic hydrophilic dye for water-based dye-sensitized solar cells. Phys. Chem. Chem. Phys. 16, 19964-19971.

Li, C.T., Lin, R.Y.Y., Lin, J.T., 2017. Sensitizers for aqueous-based solar cells. Chem. Asian J. 12, 486-496.

Lin, R.Y.Y., Wu, F.L., Li, C.T., Chen, P.Y., Ho, K.C., Lin, J.T., 2015. High-performance aqueous/organic dye-sensitized solar cells based on sensitizers containing triethylene oxide methyl ether. ChemSusChem 8, 2503-2513.

Liu, X., Gao, L., Yue, G., Zheng, H., Zhang, W, 2017. Efficient dye-sensitized solar cells incorporating hybrid counter electrode of $CuMnSnS_4$ microsperes/carbon nanotubes. Sol. Energy 158, 952-959.

Maçaira, J., Andrade, L., Mendes, A., 2017. Highly efficient $SiO_2/TiO_2$ composite photoelectrodes for dye-sensitized solar cells. Sol. Energy 158, 905-916.

Mathew, A., Anand, V., Rao, G.M., Munichandraiah, N., 2013. Effect of iodine concentration on the photovoltaic properties of dye sensitized solar cells for various $I_2$/LiI ratios. Electrochim. Acta 87, 92-96.

McConnell, I., Li, G., Brudvig, G.W., 2010. Energy conversion in natural and artificial photosynthesis. Chem. Biol. 17, 434-447.

Mengal, N., Arbab, A.A., Sahito, I.A., Memon, A.A., Sun, K.C., Jeong, S.H., 2017. An electrocatalytic active lyocell fabric cathode based on cationically functionalized and charcoal decorated graphite composite for quasi-solid state dye sensitized solar cell. Sol. Energy 155, 110-120.

Miao, L., Shi, B., Stanislaw, N., Mu, C., Qi, K., 2017. Facile synthesis of hierarchical ZnO microstructures with enhanced photocatalytic activity. Mater. Sci. - Poland 35, 45-49.

Miccoli, B., Cauda, V., Bonanno, A., Sanginario, A., Bejtka, K., Bella, F., Fontana, M., Demarchi, D., 2016. One-dimensional ZnO/gold junction for simultaneous and versatile multisensing measurements. Sci. Rep. 6, art. no. 29763.

Mohan, K., Dolui, S., Nath, B.C., Bora, A., Sharma, S., Dolui, S.K., 2017. A highly stable and efficient quasi solid state dye sensitized solar cell based on polymethyl methacrylate (PMMA)/carbon black (CB) polymer gel electrolyte with improved open circuit voltage. Electrochim. Acta 247, 216-228.

311 Park, K.H., Dhayal, M., 2015. Simultaneous growth of rutile $TiO_2$ as 1D/3D
312 nanorod/nanoflower on FTO in one-step process enhances electrochemical response of
313 photoanode in DSSC. Electrochem. Commun. 49, 47-50.

314 Paušová, Š., Kment, S., Zlámal, M., Baudys, M., Hubicka, Z., Krýsa, J., 2017.
315 Transparent nanotubular $TiO_2$ photoanodes grown directly on FTO substrates.
316 Molecules 22, art. no. 775.

317 Subramanian, S.C., Velayudhan, M.M., Narayanapillai, M., 2017. Oxa-bridged donor-
318 acceptor systems containing triazine core for dye sensitized solar cell application.
319 Chemist 90, 23-31.

320 Vekariya, R.L., Vaghasiya, J.V., Dhar, A., 2017. Coumarin based sensitizers with ortho-
321 halides substituted phenylene spacer for dye sensitized solar cells. Org. Electron. 48,
322 291-297.

323 Xiang, W., Huang, F., Cheng, Y.B., Bach, U., Spiccia, L., 2013. Aqueous dye-
324 sensitized solar cell electrolytes based on the cobalt(II)/(III) tris(bipyridine) redox
325 couple. Energy Environ. Sci. 6, 121-127.

326 Yang, C.C., Yu, Y.H., Van Der Linden, B., Wu, J.C.S., Mul, G., 2010. Artificial
327 photosynthesis over crystalline $TiO_2$-based catalysts: fact or fiction? J. Am. Chem. Soc.
328 132, 8398-8406.

329 Yang, W., Söderberg, M., Eriksson, A.I.K., Boschloo, G., 2015. Efficient aqueous dye-
330 sensitized solar cell electrolytes based on a TEMPO/$TEMPO^+$ redox couple. RSC Adv.
331 5, 26706-26709.

332 Zhu, J., Maza, W.A., Morris, A.J., 2017. Light-harvesting and energy transfer in
333 ruthenium(II)-polypyridyl doped zirconium(IV) metal-organic frameworks: a look
334 toward solar cell applications. J. Photochem. Photobiol., A 344, 64-77.